Journal of the Physical Society of Japan **89**, 094401 (2020)
https://doi.org/10.7566/JPSJ.89.094401

Horizontal Transportation of a Maltese Cross Pattern in Nematic Liquid Crystalline Droplets under a Direct-Current Electric Field

Jun Yoshioka* and Koji Fukao

Department of Physical Sciences, Ritsumeikan University, Kusatsu, Shiga 525-8577, Japan

(Received June 10, 2020; accepted July 14, 2020; published online August 19, 2020)

The deformation of director field in a nematic liquid crystalline droplet under an electric field was analyzed. In the absence of the electric field, a Maltese cross pattern was observed at the center of the droplet. Applying the electric field to the droplet, we observed that the cross pattern deformed owing to the dielectric anisotropy of the liquid crystal. In addition, under a direct-current (DC) electric field, the cross pattern moved apart from the droplet center. Flow field measurements revealed that the DC field generated a convective flow, which resulted in the movement of the pattern. Based on these results, we designed a simplified model for the flow and director fields. Using this model, we analyzed the mechanism of the director deformation based on Onsager's variational principle. Consequently, it was verified that the model, which assumes that the deformation is induced by the flow and the dielectric anisotropy, well describes the experimental results.

1. Introduction

Electrical activity with the flow of charge carriers is necessary for the maintenance of biological functions. For instance, ion pumps or ion channels control ion concentration in a cell;[1–5] rotations are driven by ion current for the synthesis of ATP in ATP synthases, and for locomotion in bacteria flagellar motors.[6–12] These biological systems can be regarded as combined systems of soft matters. Thus, the analyses for interactions between the electric field and soft matters are significant for understanding the mechanism of biological function. Focusing on the phenomena induced in the liquid crystals (which is a typical example of the soft matter) under the electric field, here we present the following two examples: the director alignment due to the dielectric anisotropy,[13–15] and the electroconvection driven by the anisotropic transportation of the charges.[13,14,16] It should be noted that both these phenomena can generate material flow, which strongly interacts with the director field.[13,14] The existence of this interaction often results in the generation of complex phenomena, such as backflow effects,[17–23] dynamic pattern formations, or the appearance of turbulence.[16,24–40]

Here we focus on the liquid crystalline (LC) droplets with several tens of micrometers, comparable to the size of the biological cells. The study of the phenomenon in the LC droplets under the electric field might help understand the mechanism of the electrical activity in the cells. In the droplets, the director field shows various configurations dependent on boundary conditions and the elastic properties with anisotropy, even in the absence of external fields.[41–54] Therefore, it is reasonably likely that in the presence of an external electric field, these droplets may exhibit various phenomena; indeed, various structural changes induced by the director alignment due to the dielectric anisotropy have been reported.[41,45,51,55–61] In contrast to these static structural change, dynamic phenomena have also been reported: the steady rotation of the director and the migration of the defects have been observed under the direct/alternating-current (DC/AC) electric fields.[62–65] The mechanisms of these phenomena would not be described only by the structural change due to the dielectric anisotropy: in addition to this, the analysis of other effects, such as the transportation of charges or material flows, would be necessary.

In this study, we analyzed the deformation of director field in the nematic liquid crystalline (NLC) droplets under the DC or AC electric field. In both cases, we observed that the Maltese cross pattern in the droplet was deformed, which indicated the deformation of the director field. However, depending on whether the applied field was DC or AC, a difference was observed in the deformation. The center of the Maltese cross pattern moved apart from the droplet center under the DC field, while stayed at the center under the AC field with high frequency. In this paper, we show that the mechanism of this phenomenon is not simply described by the director alignment due to the dielectric anisotropy: in addition to this, we need to consider the contribution from the convective flow induced by the application of the electric field.

When the deformation of the director field is induced only by the dielectric anisotropy, its mechanism is described by the competition among the conservative forces, such as the electrostatic and elastic forces. In this case, the analysis would be successfully performed by the principle of energy minimization. In contrast, when the contribution from the flow is not negligible, the principle is not applicable because the viscous force generated by the flow is non-conservative. To describe this type of phenomenon, a theory called "Onsager's variational principle" has been recently proposed.[66,67] The theory enables us to describe the non-equilibrium phenomena in soft matter systems with the framework of the variational principle. Based on this theory, we analyze the phenomenon of the structural deformation in the NLC droplet under the electric field. Moreover, we verify the validity of the analysis, via quantitative measurements for the convective flow and the change in the director field.

2. Experimental Set-up

2.1 Sample preparation

To create a system where NLC droplets are dispersed in an isotropic liquid, we mixed 7CB (Merck) and the fluorinated oligomer PF656 (OMNOVA Solution) at a weight ratio of 3 : 7. These molecules were partially mixed, and the droplets

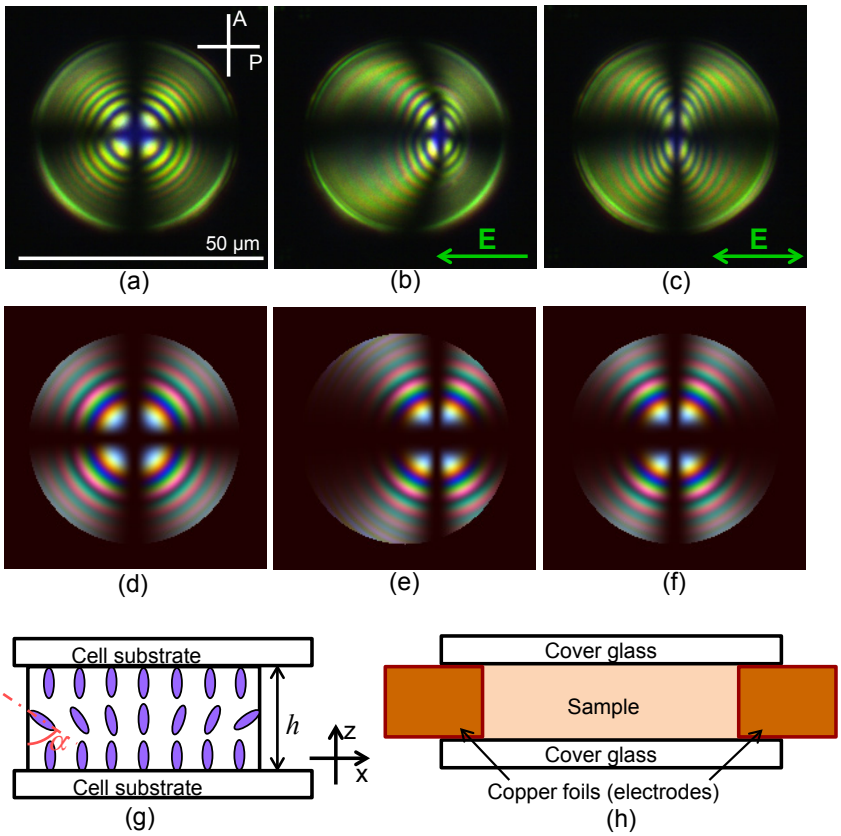

Fig. 1. (Color online) POM images of NLC droplet under DC/AC electric field. P and A in (a) indicate polarizer and analyzer respectively, and white bar 50 μm. The field is not applied in (a); DC and AC fields are applied in (b) and (c), respectively. The direction of applied DC field is shown by green arrows in (b). As the AC field, the square wave with the frequency of 1 kHz is applied. The amplitude of the electric field is 44 V/mm in (b) and (c). (d)–(f) are the light transmission intensity profiles obtained by Jones matrix calculation. As the director field, Eq. (3) is assumed in (d), Eq. (5) in (e) and Eq. (4) in (f). (g) is a schematic representation of the director field in the droplet in the absence of the electric field, and herein the physical meaning of α in Eq. (3) is illustrated. (h) is a schematic representation of a sample cell.

were formed by the cooling of the well-mixed isotropic liquid from high temperature (for more detail, see Refs. 52 and 54). This process was performed in the homemade sandwich cells described later. Spherical, spherical-cap, and cylindrical droplets were formed; however, we focused only on the cylindrical ones in this study. Moreover, for the fluorescence photo-bleaching method described in Sect. 3.2, the fluorescent dye C6-NBD ceramide (Cayman Chemical) was added to the sample at a weight ratio of 0.05%.

2.2 *Electric-field application and polarized optical microscopy*

To apply an electric field to the NLC droplets, we fabricated sandwich cells using cover-glass substrates and copper-foil spacers. The substrates were coated with the polyimide JALS204 (Japan Synthetic Rubber) to induce a homeotropic anchoring condition. The distance between the two copper foils was ~0.5–1 mm, and their thickness was 20 μm, which determined the height of the cylindrical droplet h [$h = 20$ μm, see also Fig. 1(g)]. The foils were connected to a function generator and an amplifier, to apply the DC or AC electric field to the NLC droplets.

After inserting the sample mixtures into the cells via capillary suction, we observed them by polarized optical microscopy (POM), which was performed by a commercial upright microscope of ECLIPSE LV100POL (Nikon). The observations were performed at room temperature.

2.3 *Fluorescence photo-bleaching method*

We used the fluorescence photo-bleaching method to measure the flow field.[68,69] Accordingly, we used a fluorescence microscope [ECLIPSE Ti-U (Nikon)] and an INFINITY3S-1UR CCD camera (Lumenera). The light source for the fluorescence observation and photo-bleaching was a mercury lamp. The irradiation intensity of the lamp was controlled by neutral density (ND) filters. We bleached the sample with a line pattern using a homemade slit with a width of ~200 μm. Based on the time evolution of the fluorescence images after photo-bleaching, the distribution of the flow velocity was analyzed. The detailed procedure of the bleaching method was described in Refs. 68 and 69.

2.4 *Calculations*

Analytical calculations were performed with the commercial software Mathematica (Wolfram Research), and three-dimensional drawings of the director and flow fields based on trial functions were created using the freely available software POV-Ray. Optical simulation of the POM images was performed by the Jones matrix method.[70] Based on the trial functions of the director, we calculated two-dimensional profiles of light transmission intensity under the crossed polarizer (for more details, see Ref. 52).

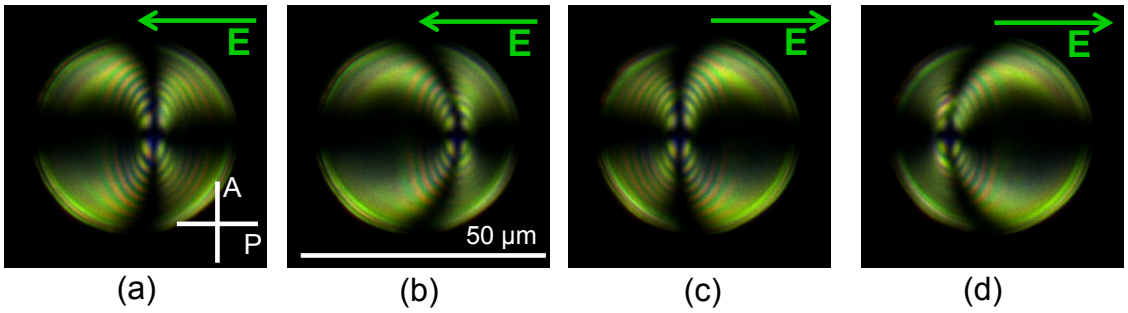

Fig. 2. (Color online) Time evolution of POM image of NLC droplet under AC electric field with low frequency. P and A in (a) indicate polarizer and analyzer respectively, and white bar 50 μm. The square wave is applied, and its amplitude and frequency are 66 V/mm and 0.1 Hz, respectively. The time interval of each image is 2.5 s. The corresponding video is available in Supplementary Material 1.[71)]

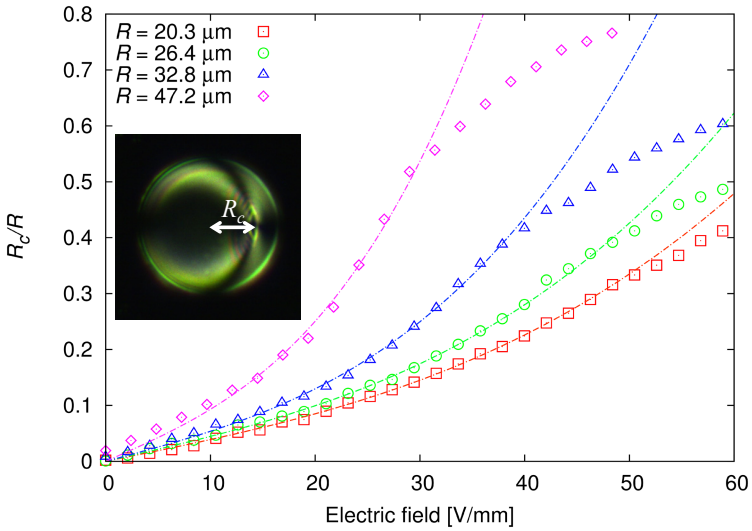

Fig. 3. (Color online) Dependence of R_c/R with the electric field E and the droplet radius R. The inset shows the schematic image of the definition of R_c.

3. Experimental Results

3.1 Director deformation under an electric field

In the cylindrical NLC droplet, a Maltese-cross pattern was observed, as shown in Fig. 1(a); similar pattern was reported in Ref. 69. When a DC electric field was applied, the center of the cross pattern moved from the droplet center to the positive electrode side [Fig. 1(b)]. On the other hand, under an AC field with relatively high frequency ($\gtrsim$10 Hz), the cross pattern stayed at the droplet center, while the texture was deformed from that in the absence of the electric field [Fig. 1(c)]. Although the four-hold rotational symmetry of the pattern was broken, two-fold symmetry was preserved in this deformation, different from the deformation under the DC field. When the AC field with low frequency was applied ($\lesssim$10 Hz), the moving direction of the Maltese cross pattern periodically changed depending on the direction of the electric field, as shown in Fig. 2 or in Supplemental Material 1.[71)] From these results, it is confirmed that the pattern tends to move to the positive electrode side, while the motion of the cross pattern cannot follow the change in the electric field with high frequency.

Focusing on the deformation of the director field under the DC electric field, we defined R_c as the distance between the center of the cross pattern and the droplet center (see the inset of Fig. 3). Normalizing R_c by the droplet radius R, we measured the dependence of R_c/R on the amplitude of the DC electric field E. As shown in Fig. 3, R_c/R increased monotonically with E in a nonlinear fashion. In addition, R_c/R monotonically increased with R.

3.2 Flow-field induced by an electric field

We measured the flow field in the droplet under the DC electric field, with using the fluorescence photo-bleaching method.[68,69)] In the process of photo-bleaching, a straight-line region of the sample was illuminated by a strong light; however, the bleached pattern showed the bended shape as shown in Figs. 4(a)–4(c). This indicates that the dyes flowed, owing to the existence of the flow field. From the time evolution of the fluorescence images, we obtained the flow distribution shown by Figs. 4(d) and 4(e). Setting y axis to be perpendicular to the direction of the electric field, we found that dependence of the flow velocity on the coordinate y was well fitted with a quadratic function of y [Fig. 4(e)]. These behaviors are quite similar with that observed in the LC droplet under the temperature gradient in Refs. 69 and 72.

Defining v_c as the flow velocity at the droplet center, we measured the dependences of v_c on the electric field E and the droplet radius R. Consequently, it was found that v_c was proportional to both E and R as shown in Figs. 5(a) and 5(b). This dependence is also similar with that in the droplets

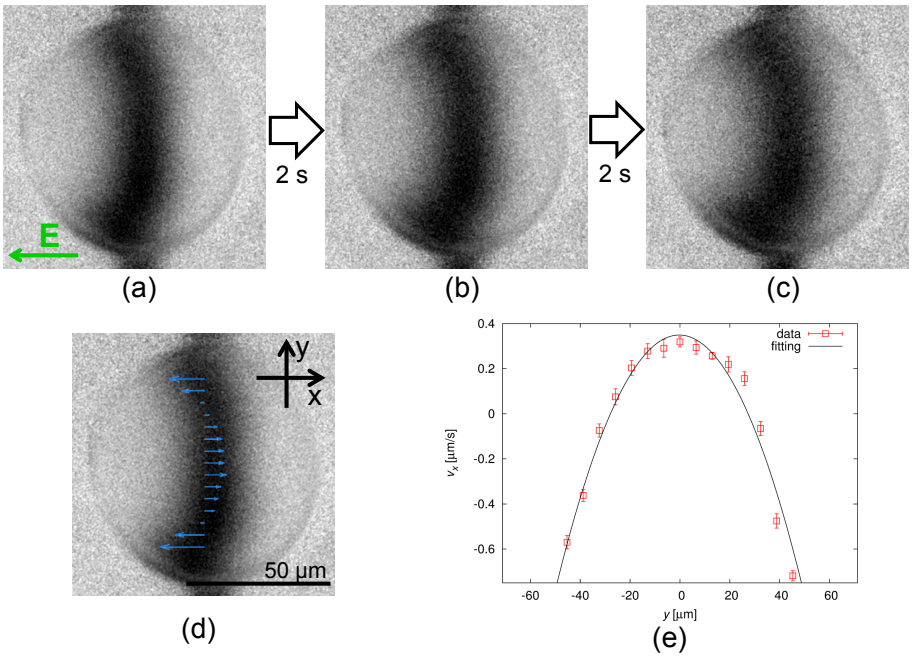

Fig. 4. (Color online) (a)–(c) Time evolution of fluorescence images of a NLC droplet after photo-bleaching. The images were normalized by the image before photo-bleaching. The green arrow in (a) indicates the direction of the DC electric field and the time interval of each image is 2 s. Applied electric field was 22 V/mm. (a) is the bleached pattern just after the photo-bleaching. The pattern is bended although a straight-line region was illuminated in the process of photo-bleaching. This is because the fluorescence dyes flow even in the bleaching process with several seconds. (d) Obtained flow velocity distribution together with the fluorescence image. (e) Dependence of the flow velocity on the coordinate y at $x = 0$. The fitting was performed with a quadratic function. Fitting errors are indicated by the error bars, which do not include experimental errors generated in the process of the sample preparation and the measurements.

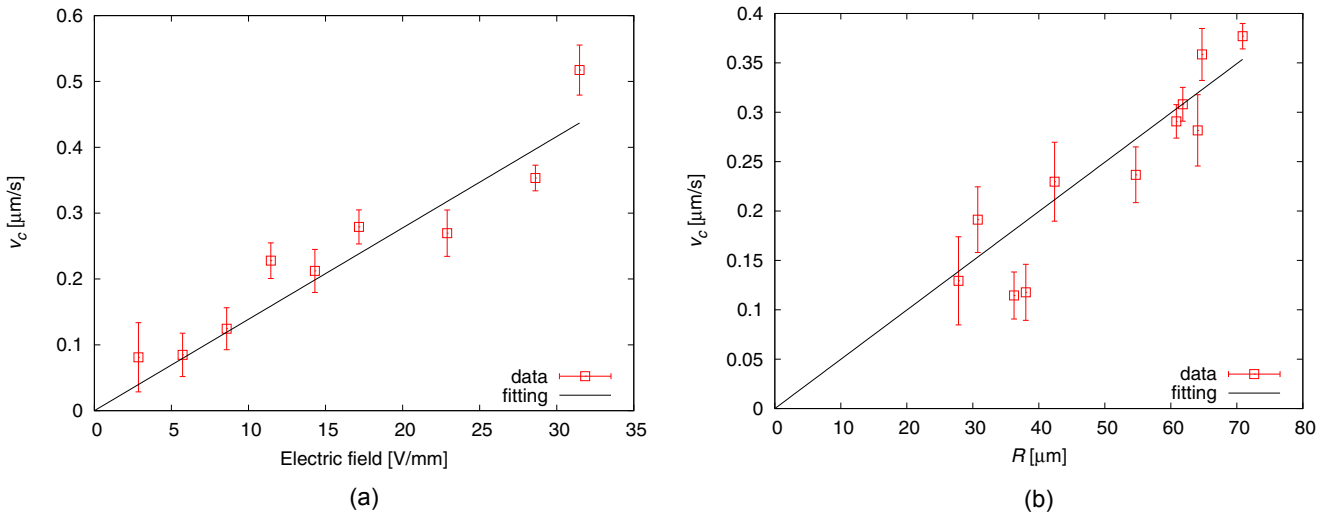

Fig. 5. (Color online) Dependence of the flow velocity on (a) applied electric field and (b) droplet radius. The flow velocity at the droplet center v_c was measured. In (a), measurement was performed in the droplet with the radius of 62 μm, and in (b), the applied electric field was 22 V/mm. Fitting errors are indicated by the error bars, which do not include experimental errors generated in the process of the sample preparation and the measurements.

under the temperature gradient: in that case, v_c was reported to be proportional to the gradient and the radius.[69,72]

In this study, we assume that the movement of the center of the Maltese cross pattern observed by POM [Fig. 1(b)] is induced by the flow described above under the DC field. On the other hand, in Sect. 3.1, we showed that the cross pattern stayed at the droplet center under the AC field with high frequency [Fig. 1(c)]. As the reason for this, the following two possibilities would be given: (i) the formation of the flow field cannot follow the high-speed change in the electric field, and (ii) the director alignment due to the viscous force cannot follow the change in the induced flow. Whatever the case, under the consideration that the structural deformation due to the flow is not effectively induced, we assume that the flow field is zero under the AC field with high frequency. Indeed, the flow as shown in Fig. 4 was not observed by the photo-bleaching method under the AC field.

Unfortunately, we could not identify the mechanism of the generation of the flow under the DC field. As mentioned in Sect. 1, it has often been reported that the electroconvection is induced in LC systems, owing to the anisotropy of the conductivity. In addition to this, in the present system, the

conductivity would not be homogeneous, since the system is the droplet surrounded by a liquid solvent. The conductivity at the interface between the droplet and the solvent (LC-solvent interface) would differ from that in the droplet. This inhomogeneity might be related to the generation of the flow. Moreover, we consider that Marangoni effect would not be negligible in the present system. Under the DC field, the distribution of the ionic impurities in the LC-solvent interface might become inhomogeneous, which would result in the appearance of the gradient in the interface tension. Indeed, as already described, it has been observed that the Marangoni flow is induced in similar systems with the present one under a temperature gradient.[54,69,72] Therefore, since we can consider various possibilities as the mechanism of the generation of the flow, it is very difficult to identify it in the present situation. We do not discuss the mechanism of the flow generation under the DC field in this paper.

4. Theoretical Analysis

As described in Sect. 3, we considered that the director deformation in the NLC droplet under the DC field would be induced owing to the dielectric anisotropy and the flow. We verify the validity of this idea by using Onsager's variational principle in this section. Based on the experimental results, the trial functions of the flow and the director fields are designed in Sects. 4.1 and 4.2, respectively. Using these functions, we analyze the present phenomenon on the basis of Onsager's variational principle in Sect. 4.3. In the end of this section, we verify whether the analysis results describe the experimental results. Finally, in Sect. 4.4, we discuss how the deformation ratio of the director field in the present phenomenon is determined on the basis of the analysis.

4.1 Simplification of flow field

As described in Sect. 3.2, since the measurement results about the flow field in the droplet under the DC electric field was similar to that under the temperature gradient in Refs. 69 and 72, we considered that the description of the flow field for these situations could be performed in a similar way. In Refs. 69 and 72, the flow field was simplified by a trial function, and we also use it in this study. The trial function is described as,

$$\begin{aligned} v_r &= \frac{V_s}{2}\left(1-\frac{r^2}{R^2}\right)\cos\phi, \\ v_\phi &= \frac{V_s}{2}\left(-1+\frac{3r^2}{R^2}\right)\sin\phi, \\ v_z &= 0, \end{aligned} \tag{1}$$

where a cylindrical coordinate (r, ϕ, z) was used. The flow field described by Eq. (1) is a convective flow as schematically illustrated in Fig. 6. The parameter V_s indicates a characteristic flow speed. In the droplet, the flow speed is maximized at two points in the LC-solvent interface with a velocity of $-V_s$, and at the droplet center, the velocity v_c is $V_s/2$. As described in Sect. 3.2, the measurement results of the flow field showed that v_c was proportional to E and R. Thus, using a constant of ζ, we can describe V_s as,

$$V_s = \zeta E R. \tag{2}$$

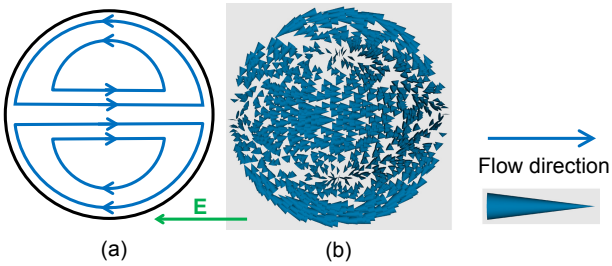

Fig. 6. (Color online) (a) Schematic illustration of the deduced flow field in the droplet under DC electric field. (b) Depiction of the flow velocity distribution based on Eq. (1). The flow direction indicated by the conical symbol in (b) is described at the right side of (b).

4.2 Simplification of director field

In the absence of the electric field, a Maltese cross pattern with four-fold rotational symmetry was observed as described in Sect. 3.1. The droplet with this pattern has already been reported in a similar experimental situation in Ref. 69, and the director field in the droplet was simplified by the following trial function:

$$\begin{aligned} (n_r, n_\phi, n_z) &= (\sin\theta_n, 0, \cos\theta_n), \\ \theta_n &= \frac{\alpha r}{R}\left(1-\frac{4z^2}{h^2}\right), \end{aligned} \tag{3}$$

where h is the height of the droplet. The central axis of the cylindrical droplet is along z axis, and the droplet center is set to be the coordinate origin. In Eq. (3), strong homeotropic anchoring condition is satisfied at the cell substrates $[(n_r, n_\phi, n_z) = (0, 0, 1)$ at $z = \pm h/2]$. θ_n indicates the polar angle of the director, and it is maximized at the LC-solvent interface in the central plane of the droplet ($r = R$, $z = 0$). The maximum value is characterized by the parameter α as shown in Fig. 1(g). When α is not zero, Eq. (3) shows a radial alignment of the director as shown in Figs. 7(a) and 7(b), and it has a circular symmetry. In this study, we assume that the director field in the absence of the electric field is described by Eq. (3). In fact, the POM image obtained by the optical simulation based on Eq. (3) is well consistent with the image observed by the experiment as shown in Figs. 1(a) and 1(d).

When the electric field is applied, the director should tend to align along the field, owing to the positive dielectric anisotropy of the NLC sample (7CB). Based on this, we considered that the director could deform as shown in Figs. 7(c) and 7(d). Such a deformation is described by the following trial function:

$$\begin{aligned} (n_r, n_\phi, n_z) &= (\sin\theta_n\cos\phi_n, \sin\theta_n\sin\phi_n, \cos\theta_n), \\ \theta_n &= \frac{\alpha r}{R}\left(1-\frac{4z^2}{h^2}\right), \\ \phi_n &= -\beta\sin 2\phi. \end{aligned} \tag{4}$$

Here, the deformation is characterized by the parameter β. In Eq. (4), the azimuthal angle of the director field is modulated from the field described by Eq. (3) with the value of ϕ_n. The absolute value of ϕ_n is maximized at the locations of $\phi = \pm\pi/4$ and $\pm 3\pi/4$; the maximum value is set as the parameter β, and when β is zero, Eq. (4) agree with Eq. (3). When β is not zero, the circular symmetry of the director field is broken, while the two-fold rotational symmetry is preserved. As

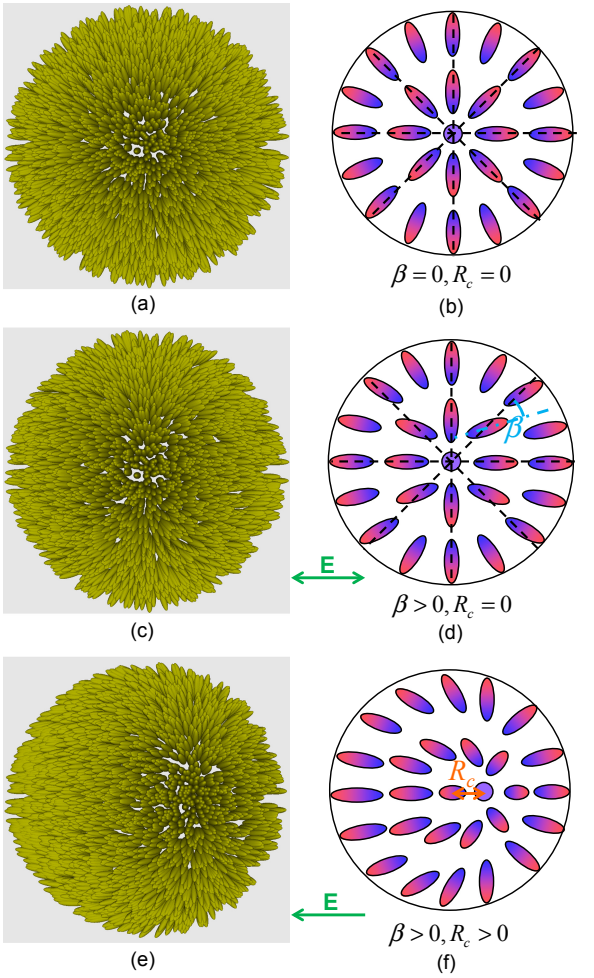

Fig. 7. (Color online) Schematic illustration of the deduced director field in the droplet. (a) and (b) represent the field in the absence of the electric field, (c) and (d) under the AC field with high frequency, and (e) and (f) under the DC field. (a), (c), and (e) are depicted based on Eqs. (3), (4), and (5), respectively. Physical meanings of β and R_c are schematically illustrated in (d) and (f), respectively.

already mentioned in Sect. 3.1, this property was also observed in the POM images under the AC electric field with high frequency; moreover, the image was well consistent with the result of the optical simulation based on Eq. (4), as shown in Figs. 1(c) and 1(f). Therefore, it is reasonable to consider that Eq. (4) well represent the director deformation in the droplet under the AC field with high frequency. Here, we can also consider that the polar angle θ_n is also influenced by the electric field. However, if we consider that α is also changed, the calculation of the Rayleighian described later becomes more complex (see Sect. 4.3). For simplicity, we assume that α is constant in this study.

Under the DC field, the center of the Maltese cross pattern moves apart from the droplet center; this indicates that the center of the radial alignment in the director field is not located at the droplet center. In addition, owing to the existence of the positive dielectric anisotropy, the director deformation described in the previous paragraph should be induced simultaneously. Therefore, we considered that the director field illustrated in Figs. 7(e) and 7(f) would be realized under the DC field. Under the assumption that the center of the radial alignment moves along the x direction, such a director field can be described by the following trial function:

$$\begin{aligned} n_r &= \frac{(r\cos\phi_n - R_c\cos(\phi-\phi_n))}{\Delta r}\sin\theta_n, \\ n_\phi &= \frac{(r\sin\phi_n + R_c\sin(\phi-\phi_n))}{\Delta r}\sin\theta_n, \\ n_z &= \cos\theta_n, \\ \Delta r &= \sqrt{r^2 + R_c^2 - 2rR_c\cos\phi}, \\ \theta_n &= \frac{\alpha\Delta r}{R}\left(1 - \frac{4z^2}{h^2}\right), \\ \phi_n &= \frac{2\beta r\sin\phi(R_c - r\cos\phi)}{\Delta r^2}, \end{aligned} \tag{5}$$

where Eq. (5) agree with Eq. (4) when R_c is zero. The POM image obtained by the optical simulation based on Eq. (5) is well consistent with the image observed by the experiment as shown in Figs. 1(b) and 1(e); thus, we considered that the simplification of the director field under the DC field would be successfully performed by Eq. (5).

4.3 *Phenomenological analysis based on Onsager's variational principle*

Using the trial functions of the flow and director fields introduced in Sects. 4.1 and 4.2 respectively, in this section, we analyze the present phenomenon based on Onsager's variational principle.[66,67] According to this theory, the state variation is determined by the minimization of the Rayleighian $\mathfrak{R}$, defined as

$$\mathfrak{R} = \frac{1}{2}W + \dot{F}, \tag{6}$$

where W is the dissipative function and $\dot{F}$ is the time derivative of the free energy F given by the total differential ($\dot{F} = \mathrm{d}F/\mathrm{d}t$). In NLC, the dissipation function per unit volume is described as,

$$w = \beta_1(e_{ij}n_in_j)^2 + \beta_2 e_{ij}^2 + \beta_3(e_{ij}n_j)^2 + \gamma_1 N_i^2 + 2\gamma_2 N_i e_{ij} n_j, \tag{7}$$

$$e_{ij} = \frac{1}{2}\left(\frac{\partial v_i}{\partial r_j} + \frac{\partial v_j}{\partial r_i}\right), \quad N_i = \frac{\mathrm{d}n_i}{\mathrm{d}t} - \frac{1}{2}\left(\frac{\partial v_i}{\partial r_j} - \frac{\partial v_j}{\partial r_i}\right)n_j, \tag{8}$$

where i and j denote the coordinates of r, ϕ, and z, and each component of the positional vector is denoted as r_i (or r_j). β_1, β_2, β_3, γ_1, and γ_2 are the viscosity coefficients,[66,67] and v_i and n_i are the flow and the director fields, respectively. Equation (7) indicates that the viscous dissipation is generated not only by the flow gradient, but also by the coupling between the flow and the director fields. Owing to the latter, the viscous force to rotate the director is induced. The effect of the director alignment induced by the flow is mainly calculated here.

We assume that the free energy is described by the summation of the elastic and the electrostatic energies:

$$F = \int (f_d + f_e)\,\mathrm{d}V, \tag{9}$$

where f_d and f_e are the elastic and the electrostatic free energy densities, respectively. These are described as,[13,14]

$$f_d = \frac{1}{2}K_1(\mathrm{div}\,\mathbf{n})^2 + \frac{1}{2}K_2(\mathbf{n}\cdot\mathrm{rot}\,\mathbf{n})^2 + \frac{1}{2}K_3|\mathbf{n}\times\mathrm{rot}\,\mathbf{n}|^2 - \frac{1}{2}(K_2+K_{24})\,\mathrm{div}(\mathbf{n}(\mathrm{div}\,\mathbf{n}) + \mathbf{n}\times\mathrm{rot}\,\mathbf{n}), \quad (10)$$

$$f_e = -\frac{1}{2}\varepsilon_0\Delta\varepsilon(\mathbf{n}\cdot\mathbf{E})^2, \quad (11)$$

where K_1, K_2, K_3, and K_{24} are the elastic constants for splay, twist, bend, and saddle-splay deformations respectively, ε_0 the dielectric constant in vacuum, $\Delta\varepsilon$ the dielectric anisotropy, and $\mathbf{E}$ the electric field. We assume that the field is uniform along the x axis:

$$(E_r, E_\phi, E_z) = (-E\cos\phi, E\sin\phi, 0). \quad (12)$$

Using Eqs. (1) and (5)–(12), we calculated the Rayleighian. Under the assumption of $K_3 \gg \varepsilon_0\Delta\varepsilon E^2h^2/10$, it is approximately calculated as,

$$\mathfrak{R} \sim \frac{\pi h\alpha^2}{15}\left[-4(\gamma_1-\gamma_2)\left(1+\frac{\beta}{2}\right)V_s\dot{R}_c + \frac{80K_3}{h^2}R_c\dot{R}_c - (\varepsilon_0\Delta\varepsilon E^2R^2 + 2(3\gamma_1-\gamma_2)V_sR_c)\dot{\beta} + 16K_2\beta\dot{\beta} + 4\gamma_1(1+\beta)\dot{R}_c^2 + \gamma_1R^2\dot{\beta}^2 + 4\gamma_1R_c\dot{R}_c\dot{\beta}\right] + \mathfrak{R}_0(R_c,\beta), \quad (13)$$

where we only showed the terms including $\dot{\beta}$ or $\dot{R}_c$, which is the time derivative of β or R_c, respectively. By minimizing Eq. (13) with respect to $\dot{\beta}$ and $\dot{R}_c$, we obtain,

$$\begin{aligned} &-(\varepsilon_0\Delta\varepsilon E^2R^2 + 2(3\gamma_1-\gamma_2)V_sR_c) + 16K_2\beta \\ &\quad + 2\gamma_1(R^2\dot{\beta} + 2R_c\dot{R}_c) = 0, \\ &-(\gamma_1-\gamma_2)\left(1+\frac{\beta}{2}\right)V_s + \frac{20K_3}{h^2}R_c \\ &\quad + \gamma_1(2(1+\beta)\dot{R}_c + R_c\dot{\beta}) = 0, \end{aligned} \quad (14)$$

where we neglected the terms higher than the first order of β or R_c. The time-independent (steady) solutions of Eq. (14) is calculated using $\dot{\beta}=0$ and $\dot{R}_c=0$. Under the assumption of $V_s^2 \gg 320K_2K_3/(h^2(\gamma_1-\gamma_2)(3\gamma_1-\gamma_2))$, the solutions are described as,

$$\beta = \frac{1}{16K_2}[\varepsilon_0\Delta\varepsilon E^2R^2 + 2(3\gamma_1-\gamma_2)V_sR_c], \quad (15)$$

$$\frac{R_c}{R} \sim \frac{(\gamma_1-\gamma_2)V_sh^2}{20K_3R}\left(1+\frac{\varepsilon_0\Delta\varepsilon E^2R^2}{32K_2}\right) = AE + BE^3, \quad (16)$$

$$A = \frac{(\gamma_1-\gamma_2)\zeta h^2}{20K_3}, \qquad B = \frac{(\gamma_1-\gamma_2)\zeta h^2\varepsilon_0\Delta\varepsilon}{640K_2K_3}R^2, \quad (17)$$

where Eq. (2) was used. It is also possible to obtain an approximate time-dependent solution for Eq. (14) as shown in Supplementary Material 2.[73] The solution shows a relaxation type, and it is consistent with Eqs. (15) and (16) when time t goes to infinity. As described in Eq. (16), R_c/R consists of the terms proportional to E and the cube of E. Defining the coefficients of these terms as A and B respectively, we can find that A is independent of R, while B is proportional to the square of R.

As shown in Fig. 3, the measurement results of the E dependence of R_c/R are well fit with Eq. (16) when the deformation is relatively small ($R_c/R \lesssim 0.4$). On the other hand, when the deformation is large ($R_c/R \gtrsim 0.4$), the results are deviated from Eq. (16). This would be because the terms higher than the first order of β or R_c were neglected in the calculation process. To describe the behavior for the large deformation, more complex calculations including these higher terms would be necessary. However, in other words, as long as we focus on the small deformation with $R_c/R \lesssim 0.4$, the E dependence of R_c/R is well described by Eq. (16) with a relatively simple form.

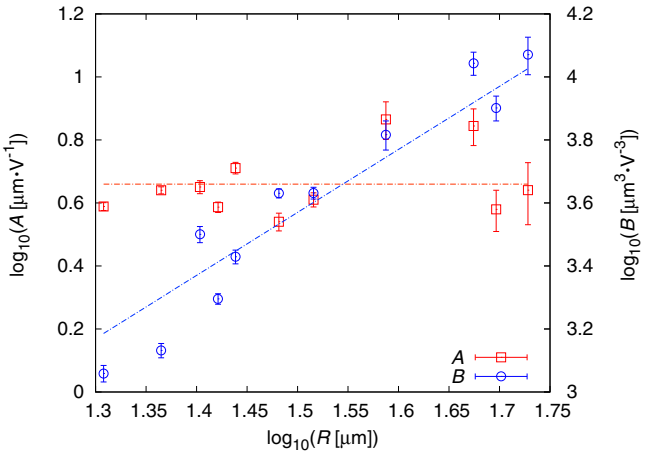

Fig. 8. (Color online) Dependence of the coefficients A and B on droplet radius R. A and B were obtained by the fitting of the measurement results using Eq. (16) (see, Fig. 3). Fitting errors are indicated by the error bars, which do not include experimental errors generated in the process of the sample preparation and the measurements. The data are shown by a double logarithmic plot, and A and B are well fitted by the lines with the slopes of 0 and 2, respectively. These are well consistent with $A \sim R^0$ and $B \sim R^2$ predicted by Eq. (17).

We obtained the R dependencies of the coefficients A and B in Eq. (16) from the fitting of the E dependence of R_c/R for small deformation. As shown in Fig. 8, in the double logarithm plots, A and B were well fitted by the lines with the slopes of 0 and 2 respectively, which were consistent with $A \sim R^0$ and $B \sim R^2$ predicted by Eq. (17). This result suggests the validity of our model, where the deformation of the director field under the DC electric field is assumed to be induced by the flow and the dielectric anisotropy.

In this section, we neglected the change of θ_n, which is the polar angle of the director (see Sect. 4.2). In our model, we can discuss the change by assuming that α is time-dependent in the calculation process of the Rayleighian. In this case, we need to solve the equation for $\partial\mathfrak{R}/\partial\dot{\alpha}=0$ in addition to Eq. (14). This made the problem very complex. Fortunately, the experimental results were well described by the analysis with the assumption that α is constant, we adopted the assumption in this study.

4.4 *Discussion*

As described by Eq. (16), since R_c is proportional to V_s, our model indicates that the transportation of the Maltese cross pattern is induced by the convective flow. A similar phenomenon under convection has already been reported in Ref. 69, where the mechanism of transportation has been described by the advection of director and director rotation induced by shear flows. In the present phenomenon, our

model suggests that the transportation of the Maltese cross pattern is driven by the same mechanism with Ref. 69.

However, Eq. (16) also includes the effect of the director deformation due to the dielectric anisotropy. In the absence of this effect, R_c/R is simply proportional to E, as long as V_s is proportional to E. In contrast, the existence of the dielectric anisotropy makes the E dependence of R_c/R nonlinear, as indicated by the second term in Eq. (16). As the structural change induced by the anisotropy increases, the optimum value of R_c/R for minimizing the Rayleighian increases if we assume that V_s is constant. Therefore, as E increases, the increase of R_c/R is promoted by the deformation due to the dielectric anisotropy in addition to the increase of V_s. Consequently, R_c/R drastically increases with the increase of E with the nonlinear behavior.

The increase of R_c/R is also induced by the increase of R in addition to E, and this tendency is also observed in the parameter β as shown in Eq. (15). This is because the director deformation due to the dielectric anisotropy monotonically increases with the electric field or the droplet size. The deformation is controlled by the competition between the electrostatic and elastic free energies, where the former promotes the deformation while the latter inhibits. The electrostatic free energy F_e is proportional to the square of E and the volume of the droplet V, which is proportional to the square of the droplet radius R and the height h ($F_e \sim E^2V \sim E^2R^2h$). On the other hand, the elastic free energy F_d is proportional to the volume and the square of the gradient of the director field as described by Eq. (10). Here, since the gradient is estimated to be proportional to the inverse of R, the total elastic free energy becomes independent of R ($F_d \sim VR^{-2} \sim h$). Therefore, as the electric field or the droplet radius increases, the contribution from the electrostatic energy relatively increases compared with that from the elastic energy. Consequently, the characteristic parameter of β or R_c/R, indicating the deformation ratio of the director field, increases with the increase of E or R.

5. Conclusion

In this study, we observed the deformation of the director field in the cylindrical NLC droplets under the DC and AC electric field. In the absence of the electric field, a Maltese cross pattern was observed at the center of the droplet. When the AC field was applied with high frequency, the texture deformation was observed; however, the cross pattern stayed at the droplet center. This deformation is attributed to the director alignment due to the dielectric anisotropy of NLC. On the other hand, when the DC field was applied, the pattern moved to the positive electrode side, together with the texture deformation. Moreover, the flow field measurement revealed that the convective flow was induced in the droplet under the DC field. From these results, we considered that the transportation of the cross pattern was driven by the flow induced by the DC field.

In the present phenomenon, the application of the DC field gives two effects — the director alignment due to the dielectric anisotropy, and the generation of the convective flow. As described above, the transportation of the Maltese cross pattern is driven by the latter; however, this pattern transportation is also affected by the structural deformation owing to the former effect. Consequently, the dependence of the parameter characterizing the deformation (R_c/R) on the electric field E shows a complex nonlinear behavior, as shown in Fig. 3.

To describe the above nonlinear behavior, we designed a simplified model about the flow and the director fields as described by Eqs. (1) and (5). Assuming that the deformation is induced owing to the flow and the dielectric anisotropy, we applied Onsager's variational principle to this model. Consequently, we obtained the E dependence of R_c/R, as shown in Eq. (16), which well described the experimental results when the deformation ratio is relatively small.

We showed that the structural deformation in the NLC droplets under the DC electric field was not only described by the competition between the conservative forces, that is, the elastic and electrostatic forces: in addition to them, we also need to consider the contribution from the non-conservative force with viscous dissipation. Onsager's variational principle might effectively describe this type of non-equilibrium phenomenon. In this study, the phenomenon was well described by the principle, which suggests its effectiveness in the description of the non-equilibrium phenomenon in liquid crystalline systems.

Acknowledgement This study was supported by JSPS KAKENHI Grant Number 18K13520.

*j-yoshi@fc.ritsumei.ac.jp

1) D. C. Gadsby, Nat. Rev. Mol. Cell Biol. **10**, 344 (2009).
2) A. L. Hodgkin and A. F. Huxley, J. Physiol. **117**, 500 (1952).
3) C. M. Armstrong and F. Bezanilla, Nature **242**, 459 (1973).
4) J. C. Skou, Biochim. Biophys. Acta **23**, 394 (1957).
5) K. B. Axelsen and M. G. Palmgren, J. Mol. Evol. **46**, 84 (1998).
6) M. Yoshida, E. Muneyuki, and T. Hisabori, Nat. Rev. Mol. Cell Biol. **2**, 669 (2001).
7) J. P. Abrahams, A. G. W. Leslie, R. Lutter, and J. E. Walker, Nature **370**, 621 (1994).
8) H. Noji, R. Yasuda, M. Yoshida, and K. Kinoshita, Nature **386**, 299 (1997).
9) Y. Sowa and R. M. Berry, Q. Rev. Biophys. **41**, 103 (2008).
10) M. Silverman and M. Simon, Nature **249**, 73 (1974).
11) G. Lowe, M. Meister, and H. C. Berg, Nature **325**, 637 (1987).
12) Y. Sowa, A. D. Rowe, M. C. Leake, T. Yakushi, M. Homma, A. Ishiwata, and R. M. Berry, Nature **437**, 916 (2005).
13) P. G. de Gennes and J. Prost, *The Physics of Liquid Crystals* (Clarendon Press, Oxford, U.K., 1993) 2nd ed.
14) S. Chandrasekhar, *Liquid Crystals* (Cambridge University Press, Cambridge, U.K., 2010) 2nd ed.
15) V. Fréedericksz and V. Zolina, Trans. Faraday Soc. **29**, 919 (1933).
16) R. Williams, J. Chem. Phys. **39**, 384 (1963).
17) F. Brochard, Mol. Cryst. Liq. Cryst. **23**, 51 (1973).
18) Z. Zou, N. A. Clark, and T. Carlsson, Phys. Rev. E **49**, 3021 (1994).
19) C. Blanc, D. Svenšek, S. Žumer, and M. Nobili, Phys. Rev. Lett. **95**, 097802 (2005).
20) S. Chono and T. Tsuji, Appl. Phys. Lett. **92**, 051905 (2008).
21) I. Dierking, M. Ravnik, E. Lark, J. Healey, G. P. Alexander, and J. M. Yeomans, Phys. Rev. E **85**, 021703 (2012).
22) T. Yanagimachi, S. Yasuzuka, Y. Yamamura, and K. Saito, J. Phys. Soc. Jpn. **81**, 034601 (2012).
23) Ž. Kos and M. Ravnik, Sci. Rep. **10**, 1446 (2020).
24) P. A. Penz, Phys. Rev. Lett. **24**, 1405 (1970).
25) S. Kai and K. Hirakawa, Solid State Commun. **18**, 1573 (1976).
26) R. Ribotta, A. Joets, and L. Lei, Phys. Rev. Lett. **56**, 1595 (1986).
27) A. Joets and R. Ribotta, J. Phys. **47**, 595 (1986).
28) M. Orlik, J. Rosenmund, K. Doblhofer, and G. Ertl, J. Phys. Chem. B **102**, 1397 (1998).
29) J.-H. Huh, Y. Hidaka, and S. Kai, J. Phys. Soc. Jpn. **67**, 1948 (1998).

30) T. John, J. Heuer, and R. Stannarius, Phys. Rev. E **71**, 056307 (2005).
31) D. Wiant, J. T. Gleeson, N. Éber, K. Fodor-Csorba, A. Jákli, and T. Tóth-Katona, Phys. Rev. E **72**, 041712 (2005).
32) S. Tanaka, S. Dhara, B. K. Sadashiva, Y. Shimbo, Y. Takanishi, F. Araoka, K. Ishikawa, and H. Takezoe, Phys. Rev. E **77**, 041708 (2008).
33) K. A. Takeuchi and M. Sano, Phys. Rev. Lett. **104**, 230601 (2010).
34) Y. Sasaki, Y. Takikawa, V. S. R. Jampani, H. Hoshikawa, T. Seto, C. Bahr, S. Herminghaus, Y. Hidaka, and H. Orihara, Soft Matter **10**, 8813 (2014).
35) R. J. Mandle, E. J. Davis, C. T. Archbold, S. J. Cowling, and J. W. Goodby, J. Mater. Chem. C **2**, 556 (2014).
36) T. Narumi, Y. Mikami, T. Nagaya, H. Okabe, K. Hara, and Y. Hidaka, Phys. Rev. E **94**, 042701 (2016).
37) H. Orihara, Y. Harada, F. Kobayashi, Y. Sasaki, S. Fujii, Y. Satou, Y. Goto, and T. Nagaya, Phys. Rev. E **99**, 012701 (2019).
38) J. Baudry, S. Pirkl, and P. Oswald, Phys. Rev. E **60**, 2990 (1999).
39) S. Pirkl and P. Oswald, Liq. Cryst. **28**, 299 (2001).
40) Y. Sasaki, V. S. R. Jampani, C. Tanaka, N. Sakurai, S. Sakane, K. V. Le, F. Araoka, and H. Orihara, Nat. Commun. **7**, 13238 (2016).
41) M. Candau, P. LeRoy, and F. Debeauvais, Mol. Cryst. Liq. Cryst. **23**, 283 (1973).
42) G. E. Volovik and O. D. Lavrentovich, Sov. Phys. JETP **58**, 1159 (1983).
43) P. Drzaic, Mol. Cryst. Liq. Cryst. **154**, 289 (1988).
44) R. Ondris-Crawford, E. P. Boyko, B. G. Wagner, J. H. Erdmann, S. Žumer, and J. W. Doane, J. Appl. Phys. **69**, 6380 (1991).
45) H.-S. Kitzerow and P. P. Crooker, Liq. Cryst. **13**, 31 (1993).
46) F. Xu and P. P. Crooker, Phys. Rev. E **56**, 6853 (1997).
47) D. Seč, T. Porenta, M. Ravnik, and S. Žumer, Soft Matter **8**, 11982 (2012).
48) T. Orlova, S. J. Aßhoff, T. Yamaguchi, N. Katsons, and E. Brasselet, Nat. Commun. **6**, 7603 (2015).
49) J. Yoshioka, F. Ito, and Y. Tabe, Soft Matter **12**, 2400 (2016).
50) G. Posnjak, S. Čoper, and I. Muševič, Nat. Commun. **8**, 14594 (2017).
51) M. K. Krakhalev, A. P. Gardymova, O. O. Prishchepa, V. Y. Rudyak, A. V. Emelyanenko, J.-H. Liu, and V. Y. Zyryanov, Sci. Rep. **7**, 14582 (2017).
52) J. Yoshioka and F. Araoka, Nat. Commun. **9**, 432 (2018).
53) J. Yoshioka, P. Salamon, D. A. Paterson, J. M. D. Storey, C. T. Imrie, A. Jákli, F. Araoka, and A. Buka, Soft Matter **15**, 989 (2019).
54) P. Oswald, J. Ignés-Mullol, and A. Dequidt, Soft Matter **15**, 2591 (2019).
55) F. Xu, H.-S. Kitzerow, and P. P. Crooker, Phys. Rev. A **46**, 6535 (1992).
56) J. Ding, H. Zhang, J. Lu, and Y. Yang, Jpn. J. Appl. Phys. **34**, 1928 (1995).
57) J. Bajc and S. Žumer, Phys. Rev. E **55**, 2925 (1997).
58) A. Shabanov, V. Presnyakov, V. Zyryanov, and S. Vetrov, Mol. Cryst. Liq. Cryst. **321**, 245 (1998).
59) T. Porenta, M. Ravnik, and S. Žumer, Soft Matter **7**, 132 (2011).
60) V. Y. Rudyak, M. N. Krakhalev, V. S. Sutormin, O. O. Prishchepa, V. Y. Zyryanov, J.-H. Liu, A. V. Emelyanenko, and A. R. Khokhlov, Phys. Rev. E **96**, 052701 (2017).
61) P. Kumar, V. Sharma, C. Jaggi, and K. K. Raina, Liq. Cryst. **44**, 757 (2017).
62) N. V. Madhusudana and R. Pratibha, Liq. Cryst. **5**, 1827 (1989).
63) Y. I. Timirov, O. A. Skaldin, E. R. Basyrova, and I. R. Kayumov, Tech. Phys. Lett. **40**, 578 (2014).
64) Y. I. Timirov, O. A. Skaldin, and E. R. Basyrova, Tech. Phys. Lett. **41**, 336 (2015).
65) Y. I. Timirov, O. A. Skaldin, E. R. Basyrova, and Y. A. Lebedev, Phys. Solid State **57**, 1912 (2015).
66) M. Doi, J. Phys.: Condens. Matter **23**, 284118 (2011).
67) A. M. Sonnet and E. G. Virga, Phys. Rev. E **64**, 031705 (2001).
68) J. Yoshioka, F. Ito, Y. Suzuki, H. Takahashi, H. Takizawa, and Y. Tabe, Soft Matter **10**, 5869 (2014).
69) J. Yoshioka and K. Fukao, Phys. Rev. E **99**, 022702 (2019).
70) R. C. Jones, J. Opt. Soc. Am. **31**, 488 (1941).
71) (Supplemental Material) Observation result of NLC droplet under AC electric field with low frequency. A square wave is applied, and its amplitude and frequency are 66 V/mm and 0.1 Hz, respectively (S1.mp4).
72) J. Yoshioka and K. Fukao, J. Phys.: Condens. Matter **32**, 325102 (2020).
73) (Supplemental Material) Time dependent solution of Eq. (14) (S2.pdf).